JOURNAL OF MATERIALS SCIENCE **34** (1999) 4727–4735

The edge-cracking of AISI 304 stainless steel during hot-rolling

F. CZERWINSKI*‡, J. Y. CHO*, A. BRODTKA*, A. ZIELINSKA-LIPIEC‡, J. H. SUNWOO§, J. A. SZPUNAR*
*Department of Metallurgical Engineering, McGill University, Montreal, Que., H3A 2B2, Canada
‡Institute of Metallurgy, University of Mining and Metallurgy, Cracow, 30-059, Poland
§Atlas Stainless Steels Inc., Tracy, Que., J3R 4R4, Canada
E-mail: frankcz@minmet.lan.mcgill.ca

The hot-rolled plates of AISI 304 stainless steel, containing edge cracks of different intensities, were examined. The austenitic matrix of the steel contained small amounts of δ ferrite inhomogeneously distributed across the width and the thickness of the plate. A correlation was found between ferrite content and edge cracking: the higher the ferrite content the longer the edge cracks. Among the chemical elements present in the steel, the most critical effect on δ ferrite content was exerted by carbon and nitrogen. The longest edge cracks were observed for plates with the lowest content of carbon and nitrogen. A possible contribution of steel chemistry and heating temperature to changes in the steel phase composition and the probability of edge cracking is discussed.

1. Introduction

Hot-rolling is a common step in manufacturing the steel products. In general, austenitic stainless steels are substantially harder during hot-rolling than either ferritic or mild steels. The high strength of these steels in hot-working conditions often requires the use of high rolling temperatures to avoid excessive mill loading. In some cases their inherently low hot-ductility may lead to edge cracking and other defects [1]. There are many factors that can affect the hot ductility of steels, such as: temperature, strain rate, composition, grain size, precipitates, non-metallic inclusions and previous thermal and mechanical treatments. Hence, a true understanding of hot rolling variables and their interactions is needed to consistently produce high quality sheet.

Several extensive reviews on steel cracking in relation to the hot rolling process have been published [2–6]. It is generally agreed that grain refinement increases the rate of recrystallization and decreases the recrystallized grain size [7]. This applies to the static recrystallization between rolling passes and to the dynamic recrystallization at the high strains. Carbides and nitrides taken into solution at soaking temperatures may, during the multi-pass operation, precipitate on dislocations and in grain boundaries, strengthening the matrix and reducing the rate of recrystallization [8]. Also the non-metallic inclusions have a detrimental effect on the hot-working behaviour and the non-deformable inclusions have more serious effects than the deformable ones [9]. The second phase particles, in general, enhance recrystallization [10]. However, the presence of a duplex structure in steel can lead to a marked reduction in hot ductility. For austenitic stainless steels the presence of non-equilibrium δ ferrite at hot-rolling temperatures impairs the hot ductility, leading to the origin of cracks at the austenite/ferrite interface [11]. Previous work on both as-cast and wrought structures has shown that, depending upon temperature and ferrite morphology, a ductility trough exists at ferrite contents in the range of 15–30%, although there are findings indicating that, in practice, smaller ferrite contents can produce defective material [12].

In this paper, we analyze the role of the chemical and phase compositions of austenitic stainless steel in the edge-crack formation during hot-rolling.

2. Experimental

Plates of austenitic stainless steel after hot rolling, containing edge cracks of different intensity, were used as a research material. Specimens with a size of $20 \times 15 \times 5$ mm and located at different distances from the plate edge, were cut from each plate. The general microstructural observations were conducted using optical microscopy. To reveal δ ferrite in the austenitic matrix, the polished sections were etched in a solution composed of 8 g NaOH and 80 ml H_2O. Electrolytic etching at room temperature and a current density of 30 mA/cm^2 made the ferrite dark, while the austenite remained unattacked. The grain boundary network of austenite was revealed by etching in a solution of 10 ml nitric acid, 10 ml acetic acid, 15 ml hydrochloric acid with addition of glycerol. A quantitative analysis

TABLE I Chemical compositions of steel plates (average values in wt %)

Plate no.	Maximum crack length (mm)	C	Mn	P	S	Si	Cr	Mo	Ni	Cu	Al	Nb	N_2	$N_2 + C$
1(E)	No cracks	0.050	1.81	0.029	0.004	0.50	18.29	0.33	8.19	0.30	0.004	0.05	0.054	0.104
2(C)	6	0.062	1.68	0.028	0.003	0.56	18.43	0.33	8.26	0.26	0.003	0.03	0.055	0.117
3(K)	20	0.067	1.82	0.029	0.008	0.46	18.53	0.34	8.28	0.27	0.003	0.09	0.037	0.104
4(L)	45	0.025	0.85	0.022	0.002	0.43	18.28	0.13	11.57	0.20	0.005	0.01	0.030	0.055
5(N)	70	0.014	1.71	0.026	0.005	0.48	18.25	0.26	9.27	0.24	0.005	0.01	0.050	0.064

Other elements: Sn: 0.01; Co: 0.07–0.1; V: 0.05–0.07; Ti: 0.1–0.01; Nb: 0.1–0.01; W: 0.02–0.11.

of the ferrite content and morphology was conducted using an image analyzing computer LECO 2000. In order to examine the details of the steel microstructure, a transmission electron microscopy (TEM) was used. The phase composition of the steel was analyzed using an X-ray Rigaku diffractometer with a rotating anode and MoK_α radiation. The crystallographic texture of the steel was measured using a Siemens D500 X-ray goniometer. Pole figures were obtained using the reflection technique, up to maximum tilt of the specimen of 80° in 5° intervals.

3. Results

3.1. Chemical composition

The average chemical compositions of hot-rolled plates with different edge qualities are shown in Table I. According to the AISI standard, they correspond to austenitic grades of 304 and 304L. In order to verify the possibility of macro-segregation, the chemical composition of the steel was measured at different distances from the plate edges. In general, the content of all the major elements across the plate width was similar, with differences very often below the accuracy level of the spectrometer used. This indicates that there is no evident segregation of any specific element, across the plate width.

In order to classify the plates in terms of the edge quality, the length of the cracks in direction perpendicular to the plate edge was measured. This indicator is of technological importance, since it represents a loss of steel, which has to be cut off from the hot-rolled plate before further processing. The maximum length of the edge cracks encountered in individual plates is also included in Table I. A comparison of data listed in Table I shows that plates with longer edge cracks have a lower sum of carbon and nitrogen content.

3.2. Phase composition

Stainless steels of types 304 and 304L after hot-rolling, examined at room temperature, are essentially austenitic. It is known, however, that some traces of δ ferrite might be present in their microstructure along with the austenite. In the first approximation, the amount of δ ferrite can be predicted from the chemical composition of steel using the Schaeffler diagram [13]. The contents of δ ferrite, estimated from that diagram using chromium and nickel equivalents, calculated according to the formulas presented in Ref. [13], are shown

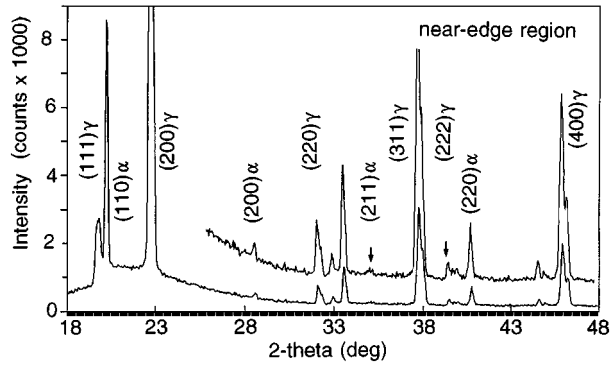

(a)

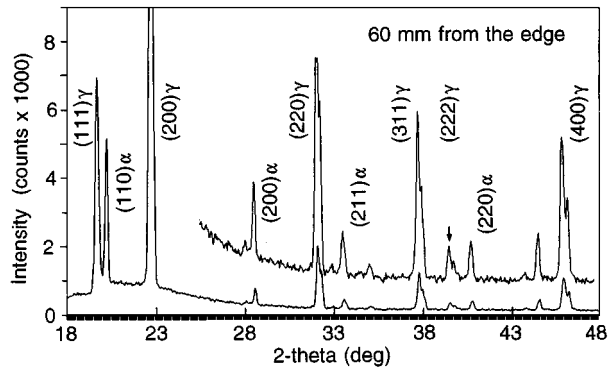

(b)

Figure 1 The X-ray diffraction patterns of the steel in the region adjacent to the plate edge (a) and the region located 60 mm from the plate edge (b). Long-term exposure using MoK_α radiation.

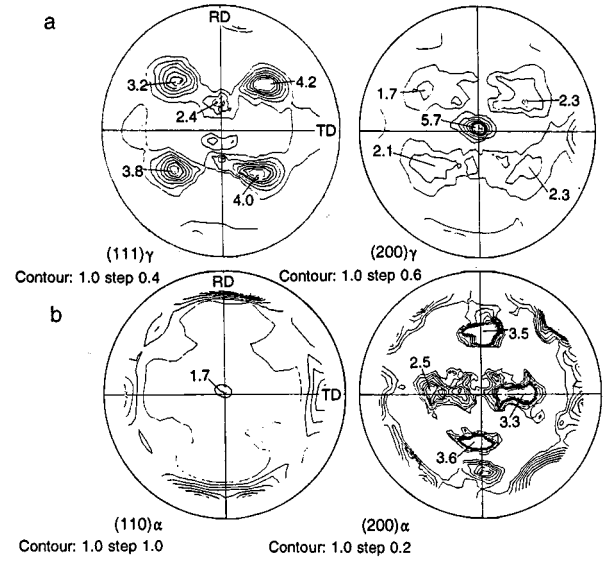

Figure 2 Pole figures of austenite (a) and ferrite (b) showing the presence of the crystallographic texture in both phases.

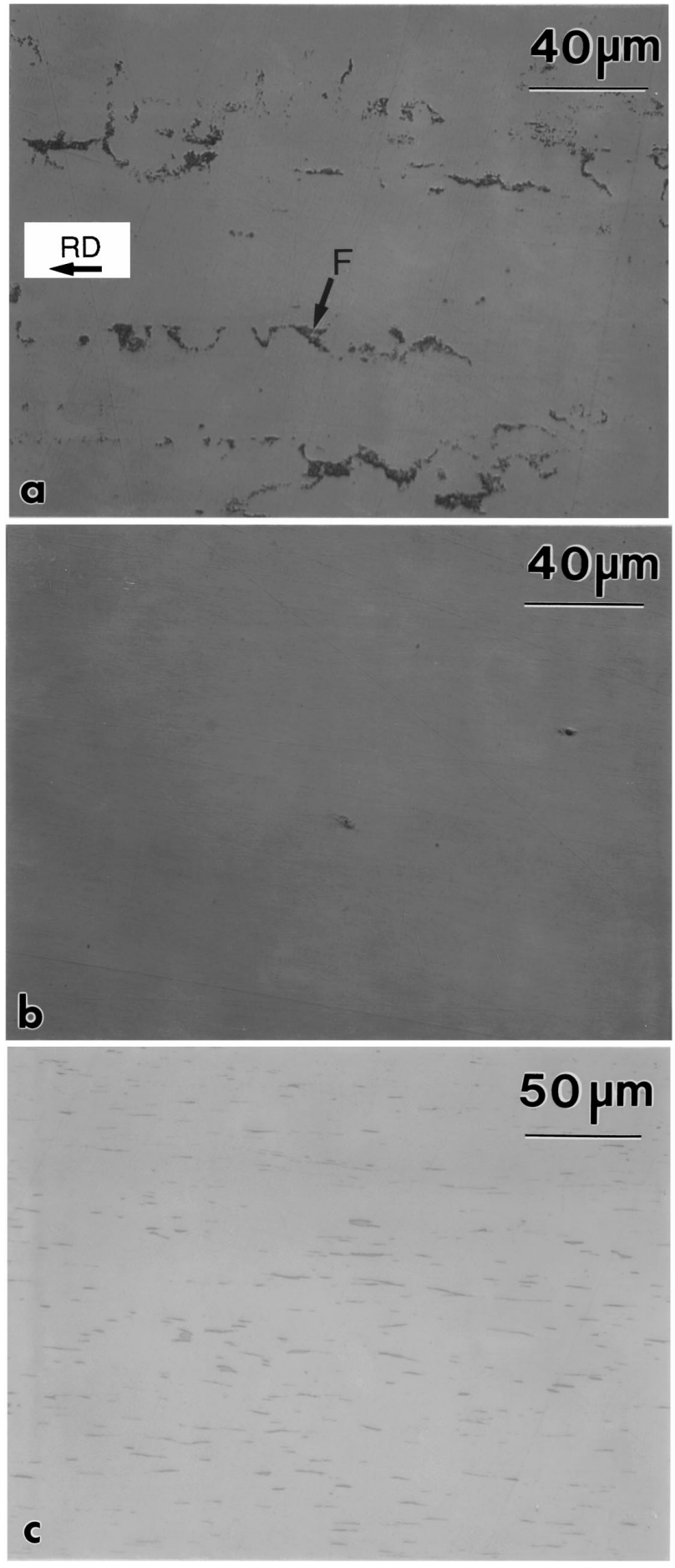

Figure 3 Optical images of the steel microstructure after etching to reveal δ ferrite: (a) plate with a maximum edge-crack length of 20 mm; (b) plate with a maximum edge-crack length of 6 mm, (a) and (b) are planar views in the rolling plane at a distance of 20 mm from the plate edge; and (c) plate with a maximum edge crack of 70 mm, cross-section view at a distance of 20 mm from the plate edge and close to the plate thickness. Rolling direction in (c) is perpendicular to the observation plane.

TABLE II The equivalents of Cr and Ni and the ferrite content estimated from the Schaeffler diagram [13]

Plate no.	Ni_{eq}[a]	Cr_{eq}[b]	Estimated ferrite content (%)
1	12.21	19.38	7
2	12.61	19.61	6
3	12.31	19.60	7
4	13.64	19.06	2
5	12.04	19.23	6

[a] $Ni_{eq} = \%Ni + 30 \times \%C + 30 \times \%N + 0.5 \times \%Mn$.
[b] $Cr_{eq} = \%Cr + \%Mo + 1.5 \times \%Si + 0.5 \times \%Nb$.

in Table II. For the plates examined, the content of δ ferrite varies between 2 and 7% and there is no clear correlation between the edge-crack length and the δ ferrite content estimated.

The presence of δ ferrite in steel plates at room temperature was confirmed by an X-ray diffraction technique. Due to a small ferrite content, long-term exposures using deep-penetrating MoK_α radiation were necessary in order to obtain clear diffraction peaks. As an example, two diffraction patterns from the same steel plate containing cracks are shown in Fig. 1. The first diffraction pattern (Fig. 1a) is from the plate-edge region and the second one (Fig. 1b) is from a region located at a distance of approximately 60 mm from the plate-edge. All the peaks of austenite and some peaks of ferrite are present and there is a substantial difference in peak intensities between both diffraction patterns. Some peaks which cannot be attributed either to ferrite or to austenite are presumably formed by trace quantities of carbides. This is in agreement with the SEM/EDX observation which revealed some chromium carbide precipitates on polished sections, in spite of a very low carbon content in the steel.

A comparison of the relative intensities of (111)γ and (110)α peaks in both diffraction patterns suggests a higher content of δ ferrite in the near-edge region. However, both the austenite (Fig. 2a) and ferrite (Fig. 2b) exhibit the crystallographic texture. This texture, according to many studies [14, 15], is in addition inhomogeneous throughout the plate width and thickness. Thus, very low intensities of ferrite peaks and the inhomogeneous texture of both phases mean that the ferrite content cannot be routinely calculated from the X-ray diffraction pattern. At this point, therefore, the X-ray diffraction data is used only as a qualitative evidence supporting the microscopic observations that indicate the ferrite phase in steel.

3.3. Distribution of δ ferrite within the steel plates

The location of δ ferrite in the steel microstructure was revealed by the metallographic technique. After electrolytic etching using a selected solution, the δ ferrite became a dark phase, while the austenitic matrix remained bright. An example of ferrite morphology revealed in two steel plates and observed in the rolling plane, is shown in Fig. 3a and b. In general, it has the appearance of islands elongated in the rolling direction. In a cross-sectional view, the thin islands of δ ferrite form a chain-like morphology (Fig. 3c). It is perhaps worth noting that the magnification of an optical microscope is not capable of revealing the detailed structure of δ ferrite which had an evident sub-structure.

A simple visual assessment of Fig. 3a and b demonstrates that the individual steel plates contained essentially different volume fractions of δ ferrite. Moreover, in each plate the distribution of δ ferrite was nonuniform. In order to provide the quantitative description of the phase segregation, the surface fraction which corresponds to the volume fraction [16] of δ ferrite was measured using automatic image analyzer. The ferrite content in selected plates, as measured on the plate surface and plotted as a function of the distance from the plate edge, is shown in Fig. 4a. It is clear that for all the plates, the highest ferrite concentration was detected in the plate-edge region and it decreased while moving towards the middle of the plate.

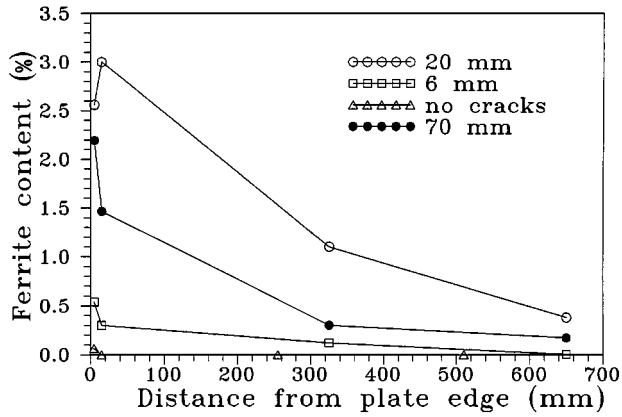

(a)

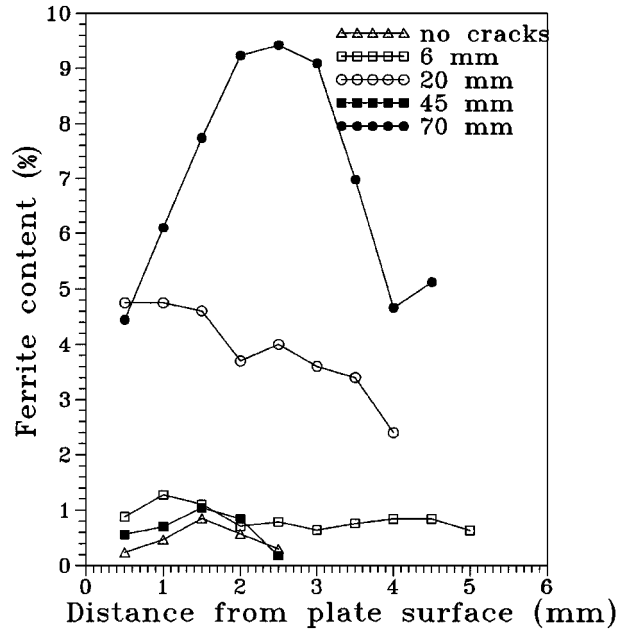

(b)

Figure 4 Stereological analysis of the distribution of δ ferrite within the steel plates: (a) change of volume fraction of δ ferrite, as measured on the plate surface, across the width of the plates with different edge cracks; and (b) change of volume fraction of δ ferrite, as measured at a distance of 20 mm from the plate edge, across the thicknesses of plates with different edge cracks.

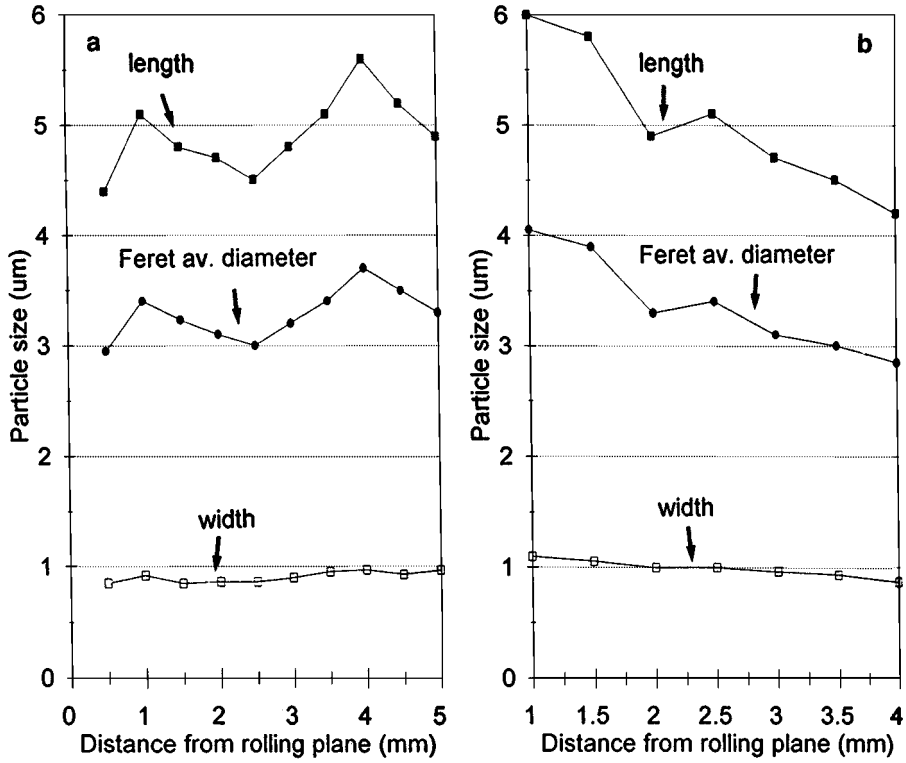

Figure 5 Stereological analysis of the changes of δ ferrite morphology across the plate thickness, (width means the size measured along the plate thickness, length means the size measured along the plate width): (a) plate with a maximum edge crack of 6 mm; and (b) plate with a maximum edge crack of 20 mm.

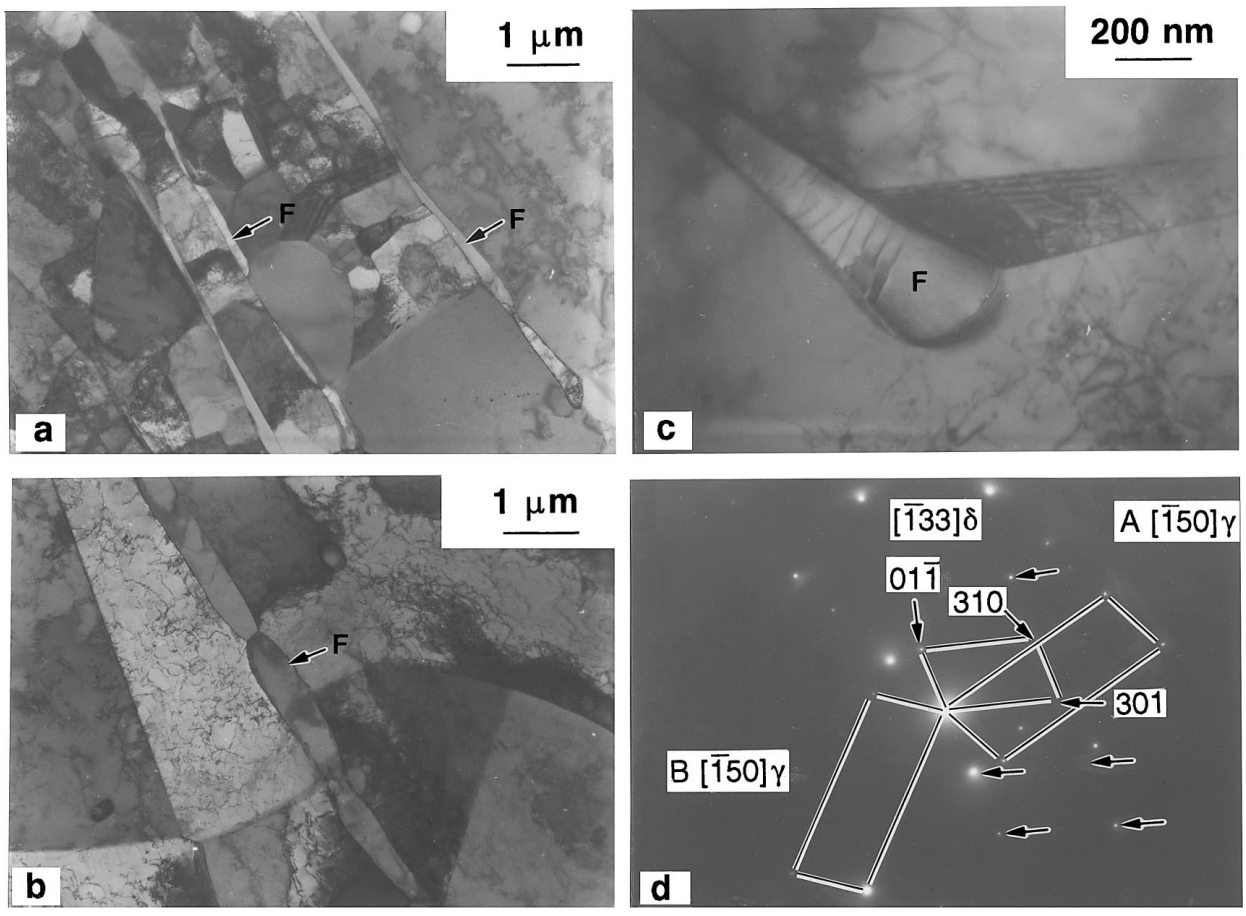

Figure 6 TEM microstructure of the plate with a maximum edge crack of 70 mm: (a) the morphology of δ ferrite in the austenitic matrix; (b) difference in dislocation density between austenite and ferrite; (c) concentration of dislocations in the vicinity of the austenite/ferrite interface; and (d) selected area electron diffraction pattern of δ ferrite with $[-133]\delta$ zone axis and austenite with two crystals A and B with $[-150]\gamma$ zone axis; individual diffraction spots of ferrite are arrowed (some of them are labelled).

In addition to segregation across the plate width, the distribution of ferrite was also nonuniform across the plate thickness of 5 mm. The plots of the volume fraction of ferrite across the plate thickness are represented by an asymmetric curve with a maximum located generally beneath the plate surface (Fig. 4b). In the case of a plate with cracks up 70 mm, the maximum volume fraction of ferrite is located in the middle of the plate thickness and is almost five times larger than that evaluated from the plate surface. In contrast, for plates containing cracks up to 20 mm in length, the ferrite concentration distribution is asymmetric and decreases gradually across the thickness from one plate surface to the other. Furthermore, the changes in ferrite content are accompanied by the variations in ferrite morphology. The cross-thickness distributions of some parameters describing ferrite morphology [16, 17] are shown in Fig. 5a and b. In general, the higher volume fraction of ferrite is accompanied by large grain size.

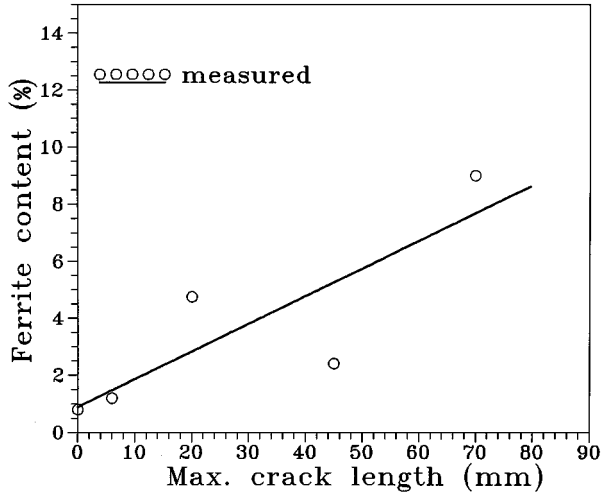

Figure 7 Relationship between the maximum edge-crack length and the maximum volume fraction of δ ferrite present within the steel plates.

3.4. TEM analysis of the morphology of δ ferrite

Additional observations were performed using TEM and a selected-area electron diffraction in order to assess more precisely both the morphology and the location of δ ferrite within the austenitic matrix. A typical microstructure of steel after hot rolling, observed on thin foils oriented perpendicular to the rolling direction, is shown in Fig. 6a. It is clear that the optical micrographs, presented in Fig. 3, did not reveal the morphology of the individual grains of δ ferrite. Some δ ferrite islands observed as dark areas in optical micrographs are not homogeneous and are composed of numerous individual ferrite grains which separate the austenitic matrix. It is interesting to note that austenite trapped in some areas between ferrite has a grain size significantly smaller than that observed in other areas.

A comparison of the austenite and δ ferrite structures indicates a higher density of dislocations in austenite than in ferrite (Fig. 6b). The additional details of the steel microstructure in two phase regions are revealed at high magnification (Fig. 6c). The high concentration of dislocations in the vicinity of the austenite/ferrite interface supports the difference in the deformation of both phases. It is generally agreed that such inhomogeneity in the microstructure may cause the generation of cavities at the austenite/ferrite interface which, in turn, may contribute to the crack's origin.

3.5. Relationship between the edge-cracking and the content of δ ferrite

The cracking of the investigated steel plates was characterized by the value of the longest crack formed during hot rolling, as measured perpendicular to the plate edge. As explained previously, this value represents the amount of steel which has to be cut-off before further processing. Fig. 7 shows the relationships between crack length and the content of δ ferrite in the steel microstructure. As a parameter which expresses the ferrite content, the maximum volume fraction, as measured metallographically on a cross-section in the plate-edge region, was taken. For each plate, the δ ferrite content was also estimated using the Schaeffler diagram [13] and the chemical composition of the particular steel specimen in plate-edge zone. These values are listed in Table II. Although to obtain a statistically reliable conclusion, a much greater amount of experimental data is required, the graph obtained from the analysis of several plates suggests a correlation between the content of δ ferrite measured in the near-edge region and the edge-crack length. It is interesting to note that in plates with longer cracks, the measured ferrite contents are close to values predicted from the chemical composition of steel (Table II). At the same time, for plates with cracks below 6 mm, the percentage of predicted ferrite (6%) does not agree with the value (0.8–1.2%) obtained in the experiments.

3.6. Analysis of cracks in steel plates

The microscopic analysis of the steel microstructure in the regions adjacent to the cracks was performed in order to assess the location of the cracks with respect to δ ferrite islands and the network of the grain boundaries of austenite. Since the surfaces of the large and open cracks were heavily oxidized at hot-rolling temperatures, they were not useful for fractographic analysis. Therefore our effort was focused on tiny branches of microcracks which surround the major cracks and penetrate deeper into the steel plate than it was anticipated from the macroscopical observations of the plate surface. A schematic representation of specimen cutting from the hot-rolled steel plate and the location of the observation plane, is depicted in Fig. 8a.

Fig. 8b shows the microstructure of the crack region after etching to reveal the grain boundaries of austenite. The location of the crack with respect to austenite grain boundaries indicates its transgranular character. In general, the crack path does not change its direction at the austenite grain boundaries. Moreover there is an evident dependence in alignment between the crack path

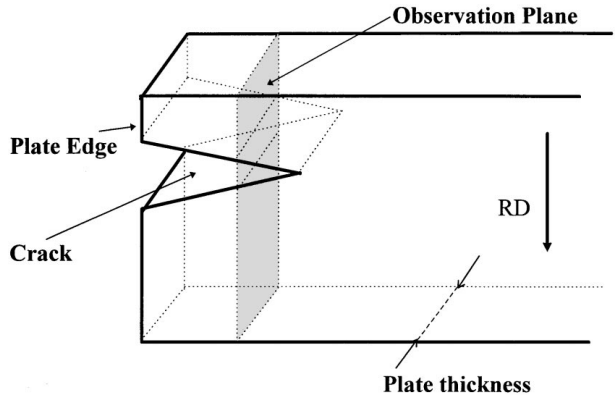

(a)

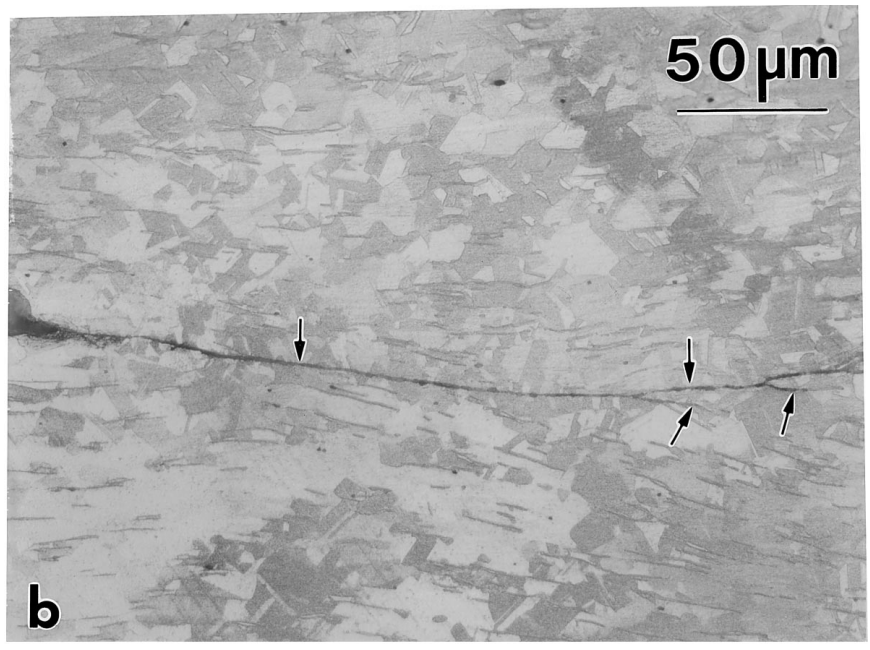

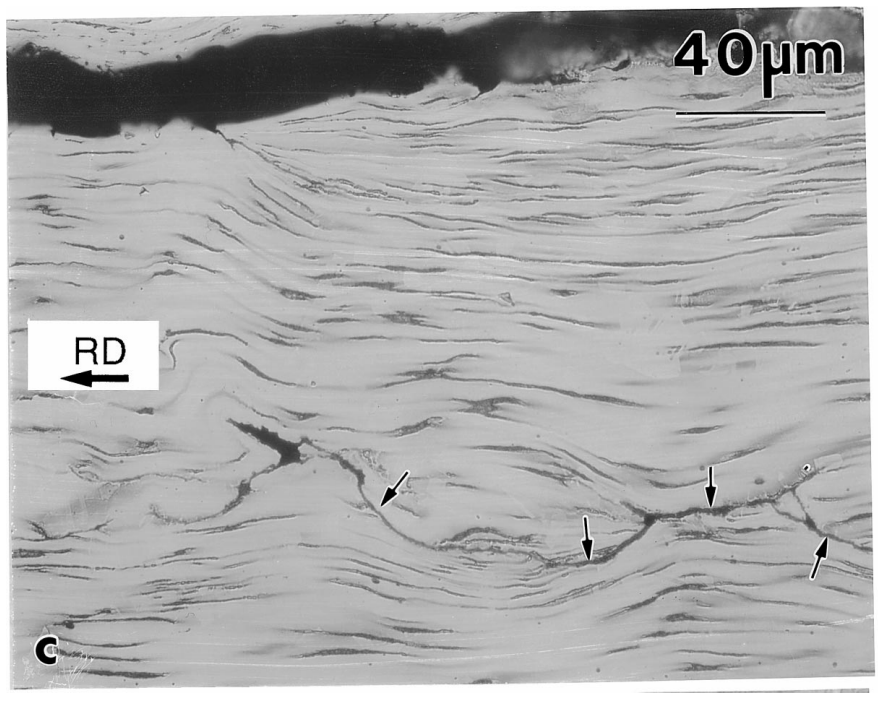

Figure 8 Optical microscopy observations of edge cracks: (a) schematic diagram of the orientation of polished sections with regard to the steel plate geometry; (b) plate microstructure after etching to reveal the grain boundary network of austenite showing the transcrystalline character of the microcrack (indicated by arrows); and (c) plate microstructure after etching to reveal δ ferrite showing the alignment of microcrack (indicated by arrows) and ferrite islands; large crack, drawn schematically in figure (a) is present in the upper part of the image.

and the δ ferrite islands. This is shown in Fig. 8c, representing the steel microstructure after etching to reveal δ ferrite. As indicated by the arrows, the cracks are situated at ferrite/austenite interfaces and then connect the neighbouring islands of ferrite through bridges of austenite.

4. Discussion

In the experimental work described above, the role of microstructure and chemical composition in edge cracking during the hot rolling of austenitic stainless steel is investigated. A major result is that the edge cracking was found to be sensitive to the content of δ ferrite. Although there is a general agreement in the literature that cracks may develop at the ferrite/austenite interface during hot rolling, the influence of δ ferrite on the hot workability of steel is considered to be more complex. According to Kane [18], the workability of 310 stainless steel ingots can be improved by certain amounts of δ ferrite. It is believed that δ ferrite retards the grain boundary migration of austenite during solidification which, in turn, leads to corrugated grain boundaries of austenite considered to be resistant to crack propagation. Moreover, the presence of the ferrite/austenite interfaces acting as nucleation sites increases the recrystallization rate. In experiments by Kane [18], cracks developed at the ferrite/austenite interface only in the cases when ferrite phase was continuous and/or temperature was low, however, they did not propagate deeply into the steel. On the other hand, there are data indicating that even small amounts of δ ferrite are critical for the hot workability of steel [12].

Three major techniques are described in the literature to measure the content of δ ferrite in steel. Apparently, the quickest and most convenient way is by using a special device called a ferroscope [19]. This technique, however, is not able to detect a microsegregation in ferrite distribution and its accuracy may be diminished by many calibrating and operating factors [20]. X-ray diffraction, although generally useful for the assessment of austenite and ferrite in steel, in this particular case cannot be routinely applied. Trace amounts of δ ferrite and the presence of preferred orientation (Fig. 2) makes X-ray data very difficult to quantify. Therefore the metallographic method was employed in this study. While supported by X-ray and TEM, this technique was found to be very precise in the assessment of δ ferrite distribution in austenitic stainless steel. Both X-ray (Fig. 1a and b) and metallographic evaluation (Fig. 4a) confirmed that there is a segregation of δ ferrite in steel plate with larger contents encountered in the plate-edge regions. Moreover, metallographic evaluation detected δ ferrite segregation across the

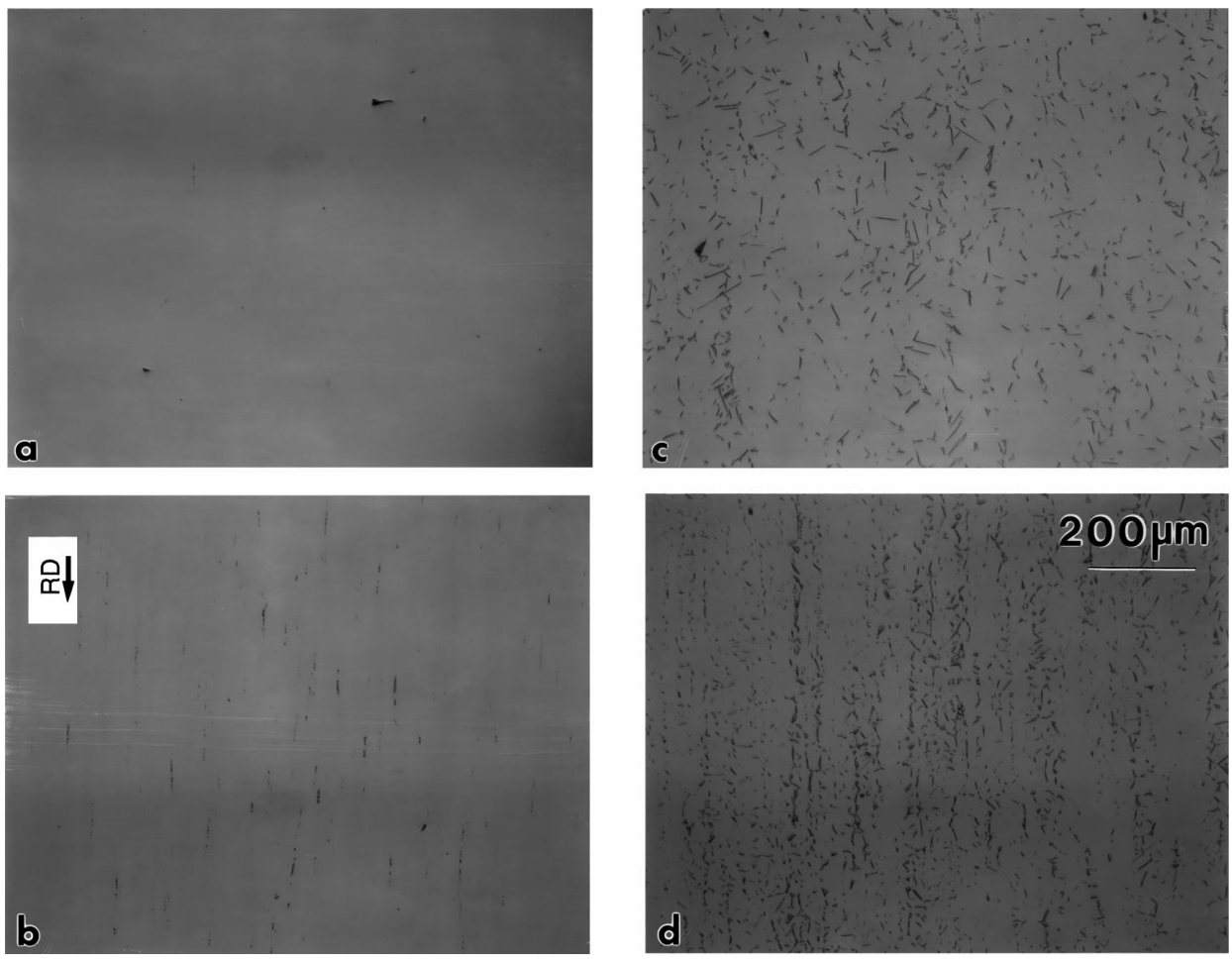

Figure 9 The influence of the annealing temperature on the ferrite content in austenitic stainless steels with different chemical composition (optical images after etching to reveal the ferrite phase): (a) steel no. 2 in Table I with a maximum sum of C + N of 0.117% annealed at 1150 °C; (b) steel no. 5 in Table I with maximum sum of C + N of 0.064% annealed at 1150 °C; (c) steel no. 2 annealed at 1350 °C; and (d) steel no. 5 annealed at 1350 °C.

plate thickness (Fig. 4b). There are two major factors which determine the steel phase composition as examined at room temperature: chemical composition and the heat treatment. Thus a lack of evident segregation of chemical elements seems to point towards the inhomogeneous temperature distribution in steel plates during pre-heating and/or hot rolling. According to the phase diagram, the higher the temperature, the higher the volume fraction of ferrite [20]. Such a simplification eliminates additional factors one of which, for example, may be the cooling rate. Namely, that the slower cooling will enhance the precipitation process and change the steel phase composition.

Although there is no significant segregation of the chemical composition within the steel plates, there are differences in the contents of some elements between individual plates. The influence of chemical composition on the content of δ ferrite should be expressed by Cr and Ni equivalents calculated according to the Schaeffler empirical formula. It is surprising that there are some discrepancies between δ ferrite content calculated (Table II) and that detected in steel plates (Fig. 7). There is, however, a dependence between edge cracking and the chemical composition, as expressed by a sum of C and N (Table I). The plates with the longest edge cracks have the lowest sum of C and N. Since both C and N enhance the formation of austenite, this finding seems to support the observation concerning the detrimental influence of δ ferrite. At this point, it should be mentioned that some other results reported in the literature claim that unstabilized nitrogen degrades hot ductility and workability in nickel based alloys and 18-8 stainless steel [18].

The research performed indicates the critical role of heating temperature and chemical composition in the formation of δ ferrite in austenitic stainless steel. In order to verify this finding and to examine the steel structures prior to hot working, samples from two plates marked as no. 2 and 5 were heat treated at 1150 and 1350 °C and subsequently water quenched. The microstructures presented in Fig. 9a–d support the findings from the analysis of hot-rolled plates. It is clear that for both annealing temperatures, the higher content of δ ferrite exists in steel no. 5 which has the longest edge cracks (Table I). The results obtained also indicate that for steels no. 2 and 5, the higher annealing temperature led to a higher content of δ ferrite.

5. Conclusions

- Hot-rolled plates of austenitic stainless steels, examined at room temperatures, contain up to 9% of δ ferrite in the austenitic matrix. The distribution of ferrite in steel plate is inhomogeneous: the highest ferrite content is located in the vicinity of the plate edge. Moreover, the content of δ ferrite changes irregularly across the plate thickness.
- The results obtained from the analysis of several plates suggest a correlation between the maximum content of δ ferrite in steel microstructure and the length of the edge-crack formed during hot-rolling; the higher the volume fraction of ferrite, the longer the edge-crack.
- Assuming that δ ferrite has an important contribution to edge cracking of steel plates at hot rolling temperatures, it can be prevented by the control of the ferrite content in the steel microstructure. The chemical composition of steel, especially contents of C and N, and the preheating temperature should be properly selected to improve the edge quality of the steel.

Acknowledgements

The authors gratefully acknowledge the financial support from Sammi Atlas Stainless Steels Inc. and from the Natural Sciences and Engineering Research Council of Canada.

References

1. C. M. SELLARS and W. J. TEGART, *Inter. Metall. Review* **17** (1972) 1.
2. W. T. LANKFORD, *Metall. Trans.* **3** (1972) 1331.
3. B. G. THOMAS, J. K. BRIMACOMBE and I. V. SAMARASEKERA, *Iron Steel Soc. Trans.* **7** (1986) 7.
4. E. T. TURKDOGAN, *AIME Steelmaking Conf. Proc.* **70** (1987) 399.
5. Y. MAEHARA, K. YASUMOTO, H. TOMONO, T. NAGAMICHI and Y. OHMORI, *Mater. Sci. Technol.* **6** (1990) 793.
6. B. MINTZ, S. YUE and J. J. JONAS, *Inter. Mater. Rev.* **36** (1991) 187.
7. K. A. BYWATER and T. GLADMAN, *Met. Technol.* **8** (1976) 358.
8. T. GLADMAN, *J. Iron Steel Inst.* **209** (1971) 380.
9. S. RUDNIK, *ibid.* **204** (1966) 374.
10. F. J. HUMPREYS and M. HATHERLY, "Recrystallization and Related Annealing Phenomena" (Pergamon Oxford, 1995).
11. K. MAYLAND, R. W. WELBURNM and A. NICHOLSON, *Met. Technol.* **8** (1976) 350.
12. J. H. DECROIX, in "Deformation Under Hot Working Conditions" (The Iron and Steel Institute, London, 1968) p. 135.
13. "Metals Handbook," 10th ed., Vol. 1 (ASM International, Materials Park, OH, 1990) p. 892.
14. D. RAABE, *Acta Mater.* **45** (1997) 1137.
15. A. J. McLAREN and C. M. SELLARS, *Mater. Sci. Technol.* **8** (1992) 1090.
16. E. E. UNDERWOOD, "Quantitative Stereology" (Addison-Wesley Publ. Co., London, 1970).
17. I. SAXL, "Stereology of Objects with Internal Structure" (Academia Praque, Praque, 1989).
18. R. H. KANE, "The Hot Deformation of Austenite" (Pergamon, 1977) p. 457.
19. "Metals Handbook," 9th ed., Vol. 17 (ASM International, Materials Park, OH, 1988) p. 129.
20. A. DESY and J. VIDTS, "Traite de metallurgie structurale" (Dunod, Paris, 1968).

Received 31 July 1998
and accepted 24 February 1999